Elephant trunk wrinkles: A mathematical model of function and form

Yang Liu* Alain Goriely[†] L. Angela Mihai[‡]

Abstract

A remarkable feature of the elephant trunk is the pronounced wrinkling that enables its great flexibility. Here, we devise a general mathematical model that accounts for characteristic skin wrinkles formed during morphogenesis in elephant trunk. Using physically realistic parameters and operating within the theoretical framework of nonlinear morphoelasticity, we elucidate analytically and numerically the effect of skin thickness, relative stiffness and differential growth on the physiological pattern of transverse wrinkles distributed along the trunk. We conclude that, since the skin and muscle components have similar material properties, geometric parameters, such as curvature, play important roles. In particular, our model predicts that, in the proximal region close to the skull, where curvature is lower, fewer wrinkles form and sooner than in the distal narrower region where more wrinkles develop. Similarly, less wrinkling is found on the ventral side, which is flatter, compared to the dorsal side. In summary, the mechanical compatibility between the skin and the muscle enables them to grow seamlessly, while the wrinkled skin acts as a protective barrier that is both thicker and more flexible than the unwrinkled skin.

Keywords: hyperelastic solids, nonlinear deformation, instabilities, wrinkling, bilayer systems, mathematical modeling.

Mathematics Subject Classification: 74B20, 74G10, 74G60, 9210.

"Elephants have wrinkles, wrinkles, wrinkles, Elephants have wrinkles, wrinkles everywhere. On their trunks, on their ears, on their knees, On their toes, no one knows, no one knows Why-I-I-I-Ih!" – Nursery Rhyme

1 Introduction

The elephant trunk (Latin proboscis, Ancient Greek $\pi\rho\sigma\gamma\sigma\sigma\kappa$ iç or proboskis) is an iconic, highly versatile limb containing approximately 100,000 radial and lateral muscles fibers, connected to the elephant's head by an opening in the skull and controlled by a proboscis nerve (Boas and Paulli, 1908; Dagenais et al., 2021; Eales, 1926; Kier and Smith, 1985). Due to its exceptional characteristics, it has attracted much interest from the research community motivated by biomimicking its properties and movements (Kaczmarski et al., 2024a,b; Leanza et al., 2024; Trivedi et al., 2008; Zhang et al., 2023).

^{*}Mathematical Institute, University of Oxford, Woodstock Road, Oxford, OX2 6GG, UK, Department of Mechanics, School of Mechanical Engineering, Tianjin University, Tianjin 300354, China

[†]Mathematical Institute, University of Oxford, Woodstock Road, Oxford, OX2 6GG, UK

[‡]Corresponding author: L.A. Mihai, Email: MihaiLA@cardiff.ac.uk, School of Mathematics, Cardiff University, Senghennydd Road, Cardiff, CF24 4AG, UK

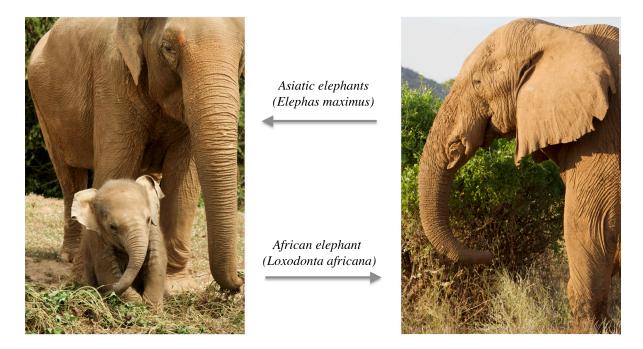


Figure 1: Elephants showing trunk wrinkles (African elephant photograph, courtesy of Zéphyr Goriely).

A salient feature contributing to elephant trunk's agility is its rich pattern of wrinkles (see Figure 1), which form and develop throughout elephant's life (Schulz et al., 2020, 2022a,b, 2023, 2024). During fetal growth, transverse trunk wrinkles and furrows appear gradually (Ayer and Mariappa, 1950; Hildebrandt et al., 2007; Schulz et al., 2024). In adult elephants, the number of transverse wrinkles differs longitudinally, with more wrinkles formed distally (at the tip) than proximally (near the skull), and more dorsal (top) than ventral wrinkles. The number of wrinkles further changes with trunk-lateralisation. MicroCT-imaging indicates that the outer trunk skin has a relatively constant thickness, while the inner skin is thinner within folds than between folds. Thus the generation of wrinkles in elephant trunk is primarily a result of differential growth appearing during development (Thompson, 1942).

Wrinkling instability is a ubiquitous mechanism involving deformations across the scales. A general theory of small strain superposed on large strain deformations for homogeneous isotropic hyperelastic materials was developed by (Green et al., 1952). Particular cases of infinitesimal deformations superposed on finite extension or compression were analyzed in (Fosdick and Shield, 1963; Wilkes, 1955; Woo and Shield, 1962). The stability of a solid circular cylinder subject to finite extension and torsion was treated in (Duka et al., 1993). For tubes of Mooney-Rivlin material with arbitrary length and thickness, by applying the Stroh formalism (Stroh, 1962), an explicit formulation for the Euler buckling load with its first nonlinear corrections was derived in (Goriely et al., 2008). A similar approach was employed in (De Pascalis et al., 2010) to calculate the nonlinear buckling load of a compressible elastic cylinder. Surface wrinkles formed by straightening of a circular sector or by bending of a cylindrical sector were examined in (Destrade et al., 2014) and (Sigaeva et al., 2018), respectively. Wrinkling due to bending of an inflated cylindrical shell was discussed in (Wu et al., 2024). An extension of Flügge's formalism (Flügge, 1962, 1973) applied to the buckling of thin-walled cylinders of nonlinear elastic material was presented in (Springhetti et al., 2023). The instability of a thick-walled hyperelastic tube subject to external pressure and axial compression was considered in (Zhu et al., 2008). Other forms of instability, like necking or bulging, also arise during inflation of elastic tubes. These phenomena were studied extensively by (Emery and Fu, 2021; Fu et al., 2016, 2021; Ilichev and Fu, 2014; Pearce and Fu, 2010; Ye et al., 2020; Wang and Fu, 2021; Wang et al., 2019). The influence of residual stresses on the stability of circular cylinders, and in particular on stretch-induced localized bulging and necking, was addressed by (Liu and Dorfmann, 2024). Post-buckling modes for a core-shell cylindrical system of neo-Hookean material under axial compression with a perfectly bonded interface were investigated experimentally, theoretically and computationally in (Zhao et al., 2014). The influence of geometrical incompatibility on pattern selection of growing bilayer tubes was modelled in (Liu et al., 2022). A cylinder with shear modulus arbitrarily varying along the radial direction which buckled and wrinkled under axial compression was examined semi-analytically in (Jia et al., 2014). The onset of wrinkling in an anisotropically growing fibre-reinforced tube was analyzed in (Ye et al., 2019). Wrinkling patterns in a cylindrical bilayer where only the outer layer grew were explored in (Jia et al., 2015). Radially distributed wrinkles induced by a thin elastic film growing on a soft elastic substrate were presented in (Jia et al., 2018).

In this paper, building on the rich methodology for elastic instabilities, we construct a mathematical model that accounts for transverse skin wrinkling in elephant trunk. Working within the theoretical framework of large strain morphoelasticity (Goriely, 2017), we address the following key question: What is the effect of the relative thickness, stiffness, and growth of the skin and muscle substrate on wrinkles formation along the elephant trunk? In Section 2, we model the trunk as a tubular cylindrical bilayer where the skin forms the thin outer layer, the muscle constitutes the thick inner layer, and a perfect bond exists between these two constituents. To account for large elastic strains, we describe each layer as an incompressible homogeneous isotropic nonlinear hyperelastic material. Assuming axisymmetric deformations, in Section 3, we present extensive numerical results for skin wrinkling when some model parameters change while others are fixed. In Section 4, we treat analytically and numerically different limiting cases. From our comprehensive analysis, we conclude that relative growth, geometry and material properties, together with loading conditions, compete to generate the characteristic pattern of transverse wrinkles in elephant trunks. While this study is motivated by a specific application scenario, our fundamental results extend further and are relevant to other applications as well.

2 Problem formulation

We model (a segment of) the elephant trunk as a cylindrical tube bilayer composed of two concentric homogeneous isotropic incompressible hyperelastic tubes. The skin forms the outer shell, while the muscle substrate constitutes the inner thicker core. We denote the reference state by \mathcal{B}_0 , and set R_0 , R_1 , h_0 and l_0 the inner and outer radii of the core, the uniform radial shell thickness, and the axial length of the cylindrical system, respectively, where $R_0 < R_1$ and $h_0 \ll R_1 - R_0$. Assuming that both the shell and the core grow until a deformed state is attained, we designate \mathcal{B} as the current configuration where the cylindrical geometry is maintained and the geometrical parameters become r_0 , r_1 , h, and l, respectively, with $r_0 < r_1$ and $h \ll r_1 - r_0$. We further assume that, at one end, the cylindrical system is fixed (homogeneous Dirichlet boundary condition), while at the other end, the system is constrained elastically (Robin boundary condition (Gustafson and Abe, 1998)) by a linear (Hookean) spring of stiffness K (Hooke's constant). Our bilayer system is represented schematically in Figure 2.

Within the usual system of cylindrical polar coordinates, we denote by $\mathbf{X} = (R, \Theta, Z)$ and

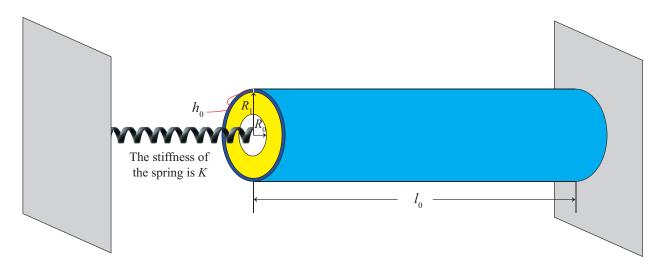


Figure 2: Schematic of the reference bilayer structure attached to a linear spring of stiffness K, with R_0 and R_1 the inner and outer radii of the core, respectively, h_0 the radial thickness of the shell, and l_0 the axial length of both the core and the shell.

 $\mathbf{x} = (r, \theta, z)$ a material point in the reference and current configuration, respectively, where

$$R_0 \leqslant R \leqslant R_1 + h_0, \qquad 0 \leqslant \Theta \leqslant 2\pi, \qquad 0 \leqslant Z \leqslant l_0,$$

$$r_0 \leqslant r \leqslant r_1 + h, \qquad 0 \leqslant \theta \leqslant 2\pi, \qquad 0 \leqslant z \leqslant l.$$

$$(2.1)$$

For both the shell and the core, the deformation gradient **F** from the reference to the current configuration takes the form (Ben Amar and Goriely, 2005; Goriely, 2017)

$$\mathbf{F} = \mathbf{AG},\tag{2.2}$$

where \mathbf{A} is the elastic deformation tensor and \mathbf{G} is the growth tensor.

Given the strain-energy function $W(\mathbf{A})$ of an incompressible homogeneous isotropic hyperelastic material, the corresponding nominal stress tensor \mathbf{S} and Cauchy stress tensor $\boldsymbol{\sigma}$ are, respectively,

$$\mathbf{S} = J\mathbf{G}^{-1}\frac{\partial W}{\partial \mathbf{A}} - pJ\mathbf{G}^{-1}\mathbf{A}^{-1} \quad \text{and} \quad \boldsymbol{\sigma} = \mathbf{A}\frac{\partial W}{\partial \mathbf{A}} - p\mathbf{I},$$
 (2.3)

where $J = \det \mathbf{F} = \det \mathbf{G}$ represents the volume change due to biological growth, p denotes the Lagrange multiplier associated with the incompressibility constraint for the isochoric elastic deformation $\det \mathbf{A} = 1$, and \mathbf{I} is the second-order identity tensor.

In the current configuration, the equilibrium equation for a quasi-static problem without body forces takes the form

$$\operatorname{div} \, \boldsymbol{\sigma} = \mathbf{0}. \tag{2.4}$$

For the axisymmetric deformation considered here, the only non-trivial equation is

$$\frac{d\sigma_{11}}{dr} + \frac{\sigma_{11} - \sigma_{22}}{r} = 0, (2.5)$$

where the indices 1, 2, 3, correspond to r-, θ -, z-directions, respectively.

In the subsequent analysis, we add the subscripts s and m to distinguish between physical quantities associated with the skin shell and the muscle core, respectively. For example, W_s represents

the strain-energy function for the skin and $W_{\rm m}$ for the muscle. Physical quantities that are valid for both these components will be written without their subscripts.

The primary deformation from \mathcal{B}_0 to \mathcal{B} is governed by the equations

$$r = r(R), \qquad \theta = \Theta, \qquad z = \lambda_z Z,$$
 (2.6)

where the longitudinal stretch ratio λ_z is constant. The deformation gradient then simplifies as follows,

$$\mathbf{F} = \frac{\mathrm{d}r}{\mathrm{d}R} \mathbf{e}_r \otimes \mathbf{e}_r + \frac{r}{R} \mathbf{e}_{\theta} \otimes \mathbf{e}_{\theta} + \lambda_z \mathbf{e}_z \otimes \mathbf{e}_z, \tag{2.7}$$

where $\{\mathbf{e}_r, \mathbf{e}_\theta, \mathbf{e}_z\}$ is the usual orthonormal basis for the coordinate system.

Denoting by $\{\lambda_i\}_{i=1,2,3}$ the principal stretch ratios in the radial, azimuthal and axial direction, respectively, by equation (2.7), we obtain

$$\lambda_1 = \frac{\mathrm{d}r}{\mathrm{d}R}, \qquad \lambda_2 = \frac{r}{R}, \qquad \lambda_3 = \lambda_z.$$
 (2.8)

We further consider the following growth tensors for the skin and muscle, respectively:

$$\begin{cases}
\mathbf{G}_{\mathrm{s}} = \mathbf{e}_{r} \otimes \mathbf{e}_{r} + \mathbf{e}_{\theta} \otimes \mathbf{e}_{\theta} + \gamma g \mathbf{e}_{z} \otimes \mathbf{e}_{z}, \\
\mathbf{G}_{\mathrm{m}} = \mathbf{e}_{r} \otimes \mathbf{e}_{r} + \mathbf{e}_{\theta} \otimes \mathbf{e}_{\theta} + g \mathbf{e}_{z} \otimes \mathbf{e}_{z},
\end{cases} (2.9)$$

where $g \ge 1$ is their common growth factor and $\gamma \ge 1$ is the differential (or relative) growth factor between the skin (outer layer) and the muscle (inner layer) in the axial (length) direction. Hence,

$$\mathbf{G}_{\mathrm{s}} = \mathbf{G}_{\gamma} \mathbf{G}_{\mathrm{m}}, \quad \text{where} \quad \mathbf{G}_{\gamma} = \mathbf{e}_{r} \otimes \mathbf{e}_{r} + \mathbf{e}_{\theta} \otimes \mathbf{e}_{\theta} + \gamma \mathbf{e}_{z} \otimes \mathbf{e}_{z}.$$
 (2.10)

From equation (2.2), we deduce that

$$\begin{cases} \mathbf{A}_{s} = \alpha_{s1}\mathbf{e}_{r} \otimes \mathbf{e}_{r} + \alpha_{s2}\mathbf{e}_{\theta} \otimes \mathbf{e}_{\theta} + \alpha_{s3}\mathbf{e}_{z} \otimes \mathbf{e}_{z}, \\ \mathbf{A}_{m} = \alpha_{m1}\mathbf{e}_{r} \otimes \mathbf{e}_{r} + \alpha_{m1}\mathbf{e}_{\theta} \otimes \mathbf{e}_{\theta} + \alpha_{m3}\mathbf{e}_{z} \otimes \mathbf{e}_{z}, \end{cases}$$

$$(2.11)$$

and, by equation (2.7), we have

$$\alpha_{m3} = \gamma \alpha_{s3} = \lambda_z g^{-1}. \tag{2.12}$$

From the incompressibility conditions det $\mathbf{A}_s = \alpha_{s1}\alpha_{s2}\alpha_{s3} = 1$ and det $\mathbf{A}_m = \alpha_{m1}\alpha_{m2}\alpha_{m3}$, together with the multiplicative decomposition (2.2), we infer that

$$\begin{cases} r \frac{\mathrm{d}r}{\mathrm{d}R} = \lambda_z^{-1} \gamma g R, & \text{for } r_1 \leqslant r \leqslant r_1 + h, \\ r \frac{\mathrm{d}r}{\mathrm{d}R} = \lambda_z^{-1} g R, & \text{for } r_0 \leqslant r \leqslant r_1. \end{cases}$$
 (2.13)

By integration, we obtain

$$\begin{cases} r^2 = \lambda_z^{-1} \gamma g(R^2 - R_1^2) + r_1^2, & \text{for } r_1 \leqslant r \leqslant r_1 + h, \\ r^2 = \lambda_z^{-1} g(R^2 - R_0^2) + r_0^2, & \text{for } r_0 \leqslant r \leqslant r_1. \end{cases}$$
(2.14)

The geometry of the system in the current configuration \mathcal{B} is described by

$$\begin{cases}
r_1 = \left[\lambda_z^{-1} g \left(R_1^2 - R_0^2\right) + r_0^2\right]^{1/2}, \\
h = \left\{\lambda_z^{-1} g \gamma \left[\left(R_1 + h_0\right)^2 - R_1^2 \right] + r_1^2 \right\}^{1/2} - r_1, \\
l = \lambda_z l_0,
\end{cases} \tag{2.15}$$

where the deformed inner radius r_0 remains to be determined.

Expressing the strain-energy function in terms of the three principal elastic stretches as $W(\alpha_1, \alpha_2, \alpha_3)$, the non-zero components of Cauchy stress tensor take the following form,

$$\begin{cases}
\sigma_{sii} = \alpha_{si} W_{si} - p_{s}, \\
\sigma_{mii} = \alpha_{mi} W_{mi} - p_{m},
\end{cases}$$
(2.16)

where $W_{\rm si} = \partial W_{\rm s}/\partial \alpha_i$ and $W_{\rm mi} = \partial W_{\rm m}/\partial \alpha_i$, i = 1, 2, 3 (there is no summation for repeated indices in the above equations). Assuming that both the outer and inner surfaces are free and the interface between the shell and the core remains continuous (perfectly bonded), we have

$$\sigma_{\text{m11}}\Big|_{r=r_0} = 0, \qquad \sigma_{\text{s11}}\Big|_{r=r_1+h} = 0, \qquad (\sigma_{\text{s11}} - \sigma_{\text{m11}})\Big|_{r=r_1} = 0.$$
 (2.17)

Since $\alpha_1\alpha_2\alpha_3 = 1$, we can define the following function depending only on two variables,

$$w(\alpha, \alpha_3) = W(\alpha_1, \alpha_2, \alpha_3), \tag{2.18}$$

where $\alpha_2 = \alpha$ and $\alpha_1 = \alpha^{-1} \alpha_3^{-1}$. Applying the chain rule, we obtain

$$w_1 = \frac{\partial w}{\partial \alpha} = \alpha^{-1}(\alpha_2 W_2 - \alpha_1 W_1), \qquad w_2 = \frac{\partial w}{\partial \alpha_3} = \alpha_3^{-1}(\alpha_3 W_3 - \alpha_1 W_1). \tag{2.19}$$

From (2.16)-(2.17), it follows that

$$\begin{cases}
\sigma_{s11} = \int_{\alpha_{h}}^{\alpha_{s}} \frac{w_{s1}}{1 - \alpha^{2} \alpha_{s3}} d\alpha, \\
\sigma_{m11} = \int_{\alpha_{r_{1}}}^{\alpha_{m}} \frac{w_{s1}}{1 - \alpha^{2} \alpha_{m3}} d\alpha + \int_{\alpha_{h}}^{\alpha_{r_{1}}} \frac{w_{s1}}{1 - \alpha^{2} \alpha_{s3}} d\alpha, \\
0 = \int_{\alpha_{r_{1}}}^{\alpha_{r_{0}}} \frac{w_{s1}}{1 - \alpha^{2} \alpha_{m3}} d\alpha + \int_{\alpha_{h}}^{\alpha_{r_{1}}} \frac{w_{s1}}{1 - \alpha^{2} \alpha_{s3}} d\alpha,
\end{cases} (2.20)$$

where

$$\alpha_{r_0} = \frac{r_0}{R_0}, \qquad \alpha_{r_1} = \frac{r_1}{R_1}, \qquad \alpha_h = \frac{r_1 + h}{R_1 + h_0}.$$
 (2.21)

In view of (2.15), the above elastic stretches are connected by

$$\begin{cases}
\alpha_{r_1}^2 = \frac{\alpha_{r_0}^2 R_0^2 + g(R_1^2 - R_0^2)}{R_1^2}, \\
\alpha_h^2 = \frac{\alpha_{r_0}^2 R_0^2 + g(R_1^2 - R_0^2) + g\gamma \left[(R_1 + h_0)^2 - R_1^2 \right]}{(R_1 + h_0)^2}.
\end{cases} (2.22)$$

The associated Lagrange multipliers can be determined from the following identities:

$$\begin{cases}
 p_{s} = \alpha_{s1} W_{s1} - \sigma_{s11}, \\
 p_{m} = \alpha_{m1} W_{m1} - \sigma_{m11}.
\end{cases}$$
(2.23)

The resultant axial force is equal to

$$N = 2\pi \left(\int_{r_0}^{r_1} \sigma_{m33} r dr + \int_{r_1}^{r_1+h} \sigma_{m33} r dr \right)$$

$$= \pi \int_{r_0}^{r_1} \left[2(\alpha_{m3} W_{m3} - \alpha_{m1} W_{m1}) - (\alpha_{m2} W_{m2} - \alpha_{m1} W_{m1}) \right] r dr$$

$$+ \pi \int_{r_1}^{r_1+h} \left[2(\alpha_{s3} W_{s3} - \alpha_{s1} W_{s1}) - (\alpha_{s2} W_{s2} - \alpha_{s1} W_{s1}) \right] r dr$$

$$= \pi R_0^2 (\lambda_z \alpha_{r_0}^2 - g) \int_{\alpha_{r_1}}^{\alpha_{r_0}} \frac{2\alpha_{m1} w_{m2} - \alpha w_{m1}}{(1 - \alpha^2 \alpha_{m3})(g - \alpha^2 \alpha_{m3})} \alpha d\alpha$$

$$+ \pi R_1^2 (\lambda_z \alpha_{r_1}^2 - g\gamma) \int_{\alpha_{r_h}}^{\alpha_{r_1}} \frac{2\alpha_{s1} w_{s2} - \alpha w_{s1}}{(1 - \alpha^2 \alpha_{s3})(g\gamma - \alpha^2 \alpha_{s3})} \alpha d\alpha. \tag{2.24}$$

Since the axial displacement is restricted at one end while the other end is attached to a spring of stiffness K, we can express the axial force as

$$N = K(l - l_0) = K(\lambda_z - 1)l_0. (2.25)$$

Then, for a given value of g, we can derive the axial extension λ_z and the deformed inner radius r_0 from the system of equations:

$$N(r_0, \lambda_z) = K(\lambda_z - 1)l_0, \qquad \sigma_{m11}(r_0, \lambda_z) = 0,$$
 (2.26)

as illustrated in Figure 3(a).

For definiteness of our problem, we consider the incompressible neo-Hookean-type functions:

$$\begin{cases}
W_{\rm s} = \frac{\mu_{\rm s}}{2} (\lambda_1^2 + \lambda_2^2 + \lambda_3^2 - 3), \\
W_{\rm m} = \frac{\mu_{\rm m}}{2} (\lambda_1^2 + \lambda_2^2 + \lambda_3^2 - 3),
\end{cases}$$
(2.27)

where $\mu_s > 0$ and $\mu_m > 0$ are shear moduli at infinitesimal strain. The respective non-dimensionalized axial Cauchy stress components are indicated in Figure 3(a).

It is useful to introduce the following dimensionless quantities:

$$\hat{R}_0 = \frac{R_0}{l_0}, \qquad \hat{R}_1 = \frac{R_1}{l_0}, \qquad \hat{h}_0 = \frac{h_0}{l_0}, \qquad \zeta = \frac{h_0}{R_1},$$
(2.28)

$$\widehat{N} = \frac{N}{\pi \mu_{\rm m} \left[(R_1 + h_0)^2 - R_0^2 \right]}, \qquad \widehat{\sigma} = \frac{\sigma}{\mu_{\rm m}}, \qquad \widehat{K} = \frac{K}{\pi \mu_{\rm m} (R_1 + h_0 + R_0)}, \qquad \beta = \frac{\mu_{\rm s}}{\mu_{\rm m}}. \quad (2.29)$$

Then, by equation (2.25), the dimensionless resultant axial force is

$$\widehat{N} = -\frac{\widehat{K}(\lambda_z - 1)}{R_1 + h_0 - R_0}. (2.30)$$

Since the skin shell is stiffer than the muscle core, surface wrinkles will be generated at some critical growth. For simplicity, henceforth, we drop the over-hat from our notation.

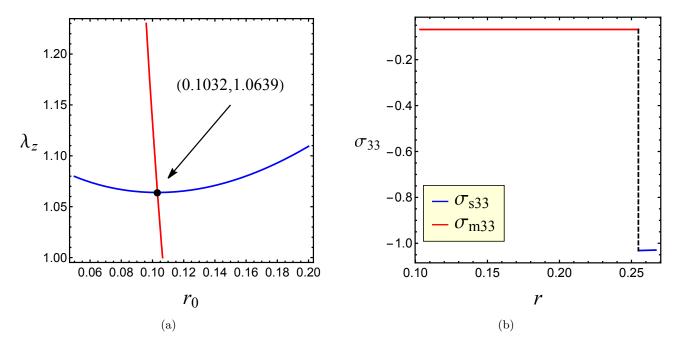


Figure 3: The non-dimensionalized (a) implicit functions of λ_z and r_0 determined by solving equations $N(r_0, \lambda_z) = -K(\lambda_z - 1)/(R_1 + h - R_0)$ (red) and $\sigma_{m11}(r_0, \lambda_z) = 0$ (blue) and (b) axial Cauchy stress σ_{33} as a function of the radius r for the skin shell (blue) and the muscle core (red) when $R_0 = 0.1$, $R_1 = 0.25$, $\zeta = 0.04$ ($h_0 = 0.01$), $\beta = 1.27$, g = 1.1, $\gamma = 1.2$, and K = 1. The dashed line in (b) indicates the stress jump across the interface $r = r_1$.

3 Linear bifurcation analysis

In this section, we derive the critical condition for transverse wrinkling (see Figure 4) using the Stroh formalism (Stroh, 1962). We then construct a robust numerical scheme using the surface impedance matrix method (Li and Yen, 1972) to solve the eigenvalue problem arising from wrinkling instability.



Figure 4: Schematic of the deformed model structure with transverse wrinkles.

3.1 Incremental theory

To obtain the incremental equations for the stability analysis, we denote the perturbed state for the bilayer system by $\widetilde{\mathcal{B}}$, with the associated position vector $\widetilde{\mathbf{x}}$. The relation between the position vectors in $\widetilde{\mathcal{B}}$ and \mathcal{B} is

$$\widetilde{\mathbf{x}}(r,z) = \mathbf{x} + \mathbf{u},\tag{3.1}$$

where $\mathbf{u} = u_1(r, z)\mathbf{e}_r + u_3(r, z)\mathbf{e}_z$ is the incremental displacement when θ is fixed. We focus on the axial instability (Zhao et al., 2014) since major wrinkles in elephant trunk tend to develop in the longitudinal direction (Schulz et al., 2024).

The deformation gradient from the reference configuration \mathcal{B}_0 to the perturbed configuration \mathcal{B} can be expressed as follows,

$$\widetilde{\mathbf{F}} = \frac{\partial \widetilde{\mathbf{x}}}{\partial \mathbf{X}} = (\mathbf{I} + \boldsymbol{\eta})\mathbf{F},$$
(3.2)

where $\eta = \operatorname{grad} \mathbf{u}$ stands for the displacement gradient given by

$$\eta = \begin{bmatrix} u_{1,1} & u_{1,2} - \frac{u_2}{r} & u_{1,3} \\ u_{2,1} & \frac{u_1}{r} + u_{2,2} & u_{2,3} \\ u_{3,1} & u_{3,2} & u_{3,3} \end{bmatrix} = \begin{bmatrix} u_{1,1} & 0 & u_{1,3} \\ 0 & \frac{u_1}{r} & 0 \\ u_{3,1} & 0 & u_{3,3} \end{bmatrix},$$
(3.3)

with $u_{i,1} = \partial u_1/\partial r$, $u_{i,2} = \partial u_1/(r\partial\theta)$, $u_{i,3} = \partial u_i/\partial z$, i = 1, 2, 3.

Assuming that the growth tensor **G** is constant, we have

$$\widetilde{\mathbf{A}}\mathbf{G} = \widetilde{\mathbf{F}} = (\mathbf{I} + \boldsymbol{\eta})\,\mathbf{F} = (\mathbf{I} + \boldsymbol{\eta})\,\mathbf{A}\mathbf{G},\tag{3.4}$$

and therefore,

$$\widetilde{\mathbf{A}} = (\mathbf{I} + \boldsymbol{\eta}) \, \mathbf{A}. \tag{3.5}$$

Recalling that the elastic deformation is isochoric, incompressibility implies $\det(\mathbf{I} + \boldsymbol{\eta}) = 1$, which in its linearized form specialises to

$$\operatorname{tr} \boldsymbol{\eta} = u_{1,1} + \frac{u_1}{r} + u_{3,3} = 0, \tag{3.6}$$

where 'tr' is the trace operator.

The nominal stress tensor in $\widetilde{\mathcal{B}}$ takes the form

$$\widetilde{\mathbf{S}} = \widetilde{J}\mathbf{G}^{-1}\frac{\partial W}{\partial \widetilde{\mathbf{A}}} - \widetilde{p}\widetilde{J}\mathbf{G}^{-1}\widetilde{\mathbf{A}}^{-1}, \tag{3.7}$$

with \widetilde{p} the associated Lagrange multiplier.

We define the Lagrange multiplier increment

$$\overline{p} = \widetilde{p} - p \tag{3.8}$$

and introduce the incremental stress tensor

$$\chi^{\mathrm{T}} = J^{-1} \mathbf{F} (\widetilde{\mathbf{S}} - \mathbf{S})^{\mathrm{T}}, \tag{3.9}$$

where 'T' denotes the transpose operator.

The incremental equilibrium equation reads

$$\operatorname{div} \boldsymbol{\chi}^{\mathrm{T}} = \mathbf{0}. \tag{3.10}$$

As the magnitude of each component of η is small, we can expand χ in terms of η , retaining the linear terms, i.e.,

$$\chi_{ij} = \mathcal{A}_{jilk} \eta_{kl} + p \eta_{ji} - \bar{p} \delta_{ji} + \mathcal{O}(|\eta_{ij}|^2), \quad i, j, k, l = 1, 2, 3,$$
(3.11)

where the summation convention for repeated indices is applied and $\mathcal{A} = (\mathcal{A}_{jilk})_{i,j,k,l=1,2,3}$ denotes the first-order instantaneous modulus tensor with the following nonzero entries:

$$\begin{cases}
\mathcal{A}_{iijj} = \alpha_i \alpha_j W_i W_j, \\
\mathcal{A}_{ijij} = \frac{\alpha_i W_i - \alpha_j W_j}{\alpha_i^2 - \alpha_j^2} \alpha_i^2, & i \neq j \text{ and } \alpha_i \neq \alpha_j, \\
\mathcal{A}_{ijij} = \frac{\mathcal{A}_{iiii} - \mathcal{A}_{jjjj} + \alpha_i W_i}{2}, & i \neq j \text{ and } \alpha_i = \alpha_j, \\
\mathcal{A}_{ijji} = \mathcal{A}_{ijij} - \alpha_i W_i, & i \neq j.
\end{cases}$$
(3.12)

Note that there is no summation for repeated indices in the above expressions and the tensor \mathcal{A} has pairwise symmetry, $\mathcal{A}_{ijkl} = \mathcal{A}_{klij}$.

By (3.3), the nonzero incremental stress components are

$$\begin{cases} \chi_{11} = \mathcal{A}_{1111}\eta_{11} + \mathcal{A}_{1122}\eta_{22} + \mathcal{A}_{1133}\eta_{33} + p \ \eta_{11} - \overline{p}, \\ \chi_{22} = \mathcal{A}_{2211}\eta_{11} + \mathcal{A}_{2222}\eta_{22} + \mathcal{A}_{2233}\eta_{33} + p \ \eta_{22} - \overline{p}, \\ \chi_{33} = \mathcal{A}_{3311}\eta_{11} + \mathcal{A}_{3322}\eta_{22} + \mathcal{A}_{3333}\eta_{33} + p \ \eta_{33} - \overline{p}, \\ \chi_{13} = \mathcal{A}_{3131}\eta_{13} + \mathcal{A}_{3113}\eta_{31} + p \ \eta_{31}, \\ \chi_{31} = \mathcal{A}_{1313}\eta_{31} + \mathcal{A}_{1331}\eta_{13} + p \ \eta_{13}. \end{cases}$$
(3.13)

Then equation (3.10) reduces to

$$\begin{cases} (r\chi_{11})_{,1} + r\chi_{13,3} - \chi_{22} = 0, \\ (r\chi_{31})_{,1} + r\chi_{33,3} = 0. \end{cases}$$
(3.14)

We emphasize that the above general formulae are valid for both the skin and muscle layers. To specify a layer, the related subscript will be added to indicate its affiliation.

The corresponding boundary and interface conditions are, respectively:

$$\chi_{\mathrm{s}} \mathbf{e}_r \Big|_{r=r_1+h} = \mathbf{0}, \qquad (\chi_{\mathrm{s}} - \chi_{\mathrm{m}}) \, \mathbf{e}_r \Big|_{r=r_1} = \mathbf{0}$$
(3.15)

and

$$(u_{s1} - u_{m1})\Big|_{r=r_1} = 0, \qquad (u_{s3} - u_{m3})\Big|_{r=r_1} = 0.$$
 (3.16)

The sliding conditions at the ends are

$$\mathbf{e}_r \cdot \boldsymbol{\chi}_s \mathbf{e}_z \Big|_{z=0,l} = 0, \qquad \mathbf{e}_r \cdot \boldsymbol{\chi}_m \mathbf{e}_z \Big|_{z=0,l} = 0.$$
 (3.17)

3.2 Stroh formulation

Employing the Stroh method (Stroh, 1962), we look for periodic solutions of the form:

$$\begin{cases} u_1(r,z) = U(r)\cos kz, & u_3(r,z) = W(r)\sin kz, \\ \chi_{11}(r,z) = T_{11}(r)\cos kz, & \chi_{31}(r,z) = T_{31}(r)\sin kz, \end{cases}$$
(3.18)

where k represents the wave number in the axial direction. In view of equations (3.13), (3.18), denoting the dimensionless wave number by n, the sliding conditions (3.17) yield

$$k = \frac{n\pi}{l}, \quad n = 1, 2, 3, \cdots$$
 (3.19)

We further define a displacement-traction vector

$$\mathbf{\Gamma} = [\mathbf{U}(r), \mathbf{T}(r)]^{\mathrm{T}}, \quad \text{with} \quad \mathbf{U}(r) = [U(r), W(r)]^{\mathrm{T}} \quad \text{and} \quad \mathbf{T}(r) = [T_{11}(r), T_{31}(r)]^{\mathrm{T}}. \tag{3.20}$$

From (3.6), (3.10), and $(3.13)_{1.5}$, we obtain

$$\mathbf{\Gamma}'(r) = \frac{1}{r} \mathbf{N}(r) \mathbf{\Gamma}(r), \tag{3.21}$$

with the prime denoting differentiation with respect to r and the Stroh block matrix taking the form

$$\mathbf{N} = \begin{bmatrix} \mathbf{N}_1 & \mathbf{N}_2 \\ \mathbf{N}_3 & -\mathbf{N}_1^{\mathrm{T}} \end{bmatrix}, \tag{3.22}$$

where N_i (i = 1, 2, 3) are 2×2 sub-matrices, such that N_2 and N_3 are symmetric. These sub-matrices can be expressed as follows,

$$\mathbf{N}_{1} = \begin{bmatrix} -1 & -rk \\ \frac{rk(\mathcal{A}_{1331} + p)}{\mathcal{A}_{1313}} & 0 \end{bmatrix}, \quad \mathbf{N}_{2} = \begin{bmatrix} 0 & 0 \\ 0 & \frac{1}{\mathcal{A}_{1313}} \end{bmatrix}, \quad \mathbf{N}_{3} = \begin{bmatrix} t_{11} & t_{12} \\ t_{12} & t_{22} \end{bmatrix}, \quad (3.23)$$

where

$$\begin{cases}
t_{11} = \mathcal{A}_{1111} - 2\mathcal{A}_{1122} + \mathcal{A}_{2222} + r^2 k^2 \mathcal{A}_{3131} - \frac{r^2 k^2}{\mathcal{A}_{1313}} (\mathcal{A}_{1331} + p)^2 + 2p, \\
t_{12} = rk \left(\mathcal{A}_{1111} - \mathcal{A}_{1122} - \mathcal{A}_{1133} + \mathcal{A}_{2233} + p \right), \\
t_{22} = r^2 k^2 \left(\mathcal{A}_{1111} - 2\mathcal{A}_{1133} + \mathcal{A}_{3333} + 2p \right).
\end{cases}$$
(3.24)

3.3 The surface impedance matrix method

Next, we apply the surface impedance matrix method (Biryukov, 1985; Biryukov et al., 1995; Shuvalov, 2003a,b), and introduce the conditional impedance matrix $\mathbf{Z}(r)$ which satisfies

$$\mathbf{T} = \mathbf{Z}(r)\mathbf{U}.\tag{3.25}$$

From the relations

$$\mathbf{U}' = \frac{1}{r}(\mathbf{N}_1 \mathbf{U} + \mathbf{N}_2 \mathbf{T}), \qquad \mathbf{T}' = \frac{1}{r}(\mathbf{N}_3 \mathbf{U} - \mathbf{N}_1^{\mathrm{T}} \mathbf{T}), \tag{3.26}$$

we obtain the Riccati equation

$$\mathbf{Z}' = \frac{1}{r} \Big(\mathbf{N}_3 - \mathbf{N}_1^{\mathrm{T}} \mathbf{Z} - \mathbf{Z} \mathbf{N}_1 - \mathbf{Z} \mathbf{N}_2 \mathbf{Z} \Big). \tag{3.27}$$

We then apply the above general expressions to the bilayer system. Fur the skin layer, we use the boundary condition $\mathbf{Z}(r_1+h)=\mathbf{0}$ determined from (3.15) to integrate (3.27) from r_1+h to r_1 and find $\mathbf{Z}_{\mathrm{s}}(r_1)$. Applying the same procedure to the muscle layer yields $\mathbf{Z}_{\mathrm{m}}(r_1)$. The displacement and traction continuities at interface results in $(\mathbf{Z}_{\mathrm{m}}(r_1) - \mathbf{Z}_{\mathrm{s}}(r_1)) \mathbf{U}_{\mathrm{s}}(r_1) = \mathbf{0}$. For surface wrinkling, the existence of a non-trivial solution of \mathbf{U} finally leads to the bifurcation condition

$$\Phi(\beta, \gamma, n, g, R_0, R_1, h_0, K) = 0, \tag{3.28}$$

where

$$\Phi(\beta, \gamma, n, g, R_0, R_1, h_0, K) = \det \left(\mathbf{Z}_{m}(r_1) - \mathbf{Z}_{s}(r_1) \right). \tag{3.29}$$

3.4 Numerical examples

In this section, the interplay between different model parameters is captured by numerical examples where some model parameters vary while others are kept fixed. For the elephant trunk, in (Schulz et al., 2022a; Wilson et al., 1991), the Young moduli of skin and muscle tissue are estimated as $E_{\rm s}=3\mu_{\rm s}\leq 1190\pm 120$ kPa and $E_{\rm m}=3\mu_{\rm m}\approx 938$ kPa, respectively, and the skin is found at most 1.27 times stiffer than the muscle. Nonetheless, we should mention that those moduli were measured by deforming wrinkled skin samples, first at small strain then at large strains, and therefore, the large strain measurements would be closer to those for the unwrinkled skin, which are not available. Additionally, these quantities will be different in the unborn elephant, where wrinkles first form (Schulz et al., 2024), than in calf and in adult elephants where wrinkles continue to evolve. Further measurements are needed. Meanwhile, our relevant plots in this paper are those where the modulus ratio is $\beta=1.27$. Notwithstanding these estimates, our modelling approach is valid more generally, and we include a wide range of examples which are valuable in their own right and can be useful to this and other applications as well.

In Figure 5, we show bifurcation curves identified from the solutions of (3.28) for different parameter values. These plots suggest that the relative growth factor γ decreases as a function of the wave number n when the pre-growth factor g increases and also when the relative modulus β increases. For each curve, the local minimum gives the first bifurcation point with the critical relative growth $\gamma_{\rm cr}$ and the critical wave number $n_{\rm cr}$. In particular, when $\beta = 1.27$, the relative growth factor $\gamma \sim 2$ appears to be optimal.

For β large, as illustrated in Figure 6(a) shows bifurcation curves, all closed curves are shrinking for increasing β , indicating a higher modulus ratio delays the critical relative growth $\gamma_{\rm cr}$. Additionally, the bifurcation condition (3.28) has no solution for some ranges of n values. This feature is quite different from the previously known result that a stiffer film triggers an earlier instability. Another inference is that, for a large enough β , the bifurcation curve may vanish. To study this feature, we plot in Figure 6(b) the function Φ , given by equation (3.29), with the differential growth factor γ increasing while n=12 and the other parameters as in Figure 6(a). The dots where the black arrow crosses the curves in Figure 6(b) highlight the minimum points, not the bifurcation points (note that the bifurcation point satisfies the bifurcation condition $\Phi = 0$). Meanwhile, the arrow indicates that all curves increase with increasing β , until a critical value $\beta_{\rm max}^{(n=12)}$, where the function Φ is tangential to the line $\Phi = 0$. When θ exceeds this value, the bifurcation condition has no solution. In general, for $n = n_{\rm cr}$, the critical value is $\theta_{\rm max}$, which gives the global maximum

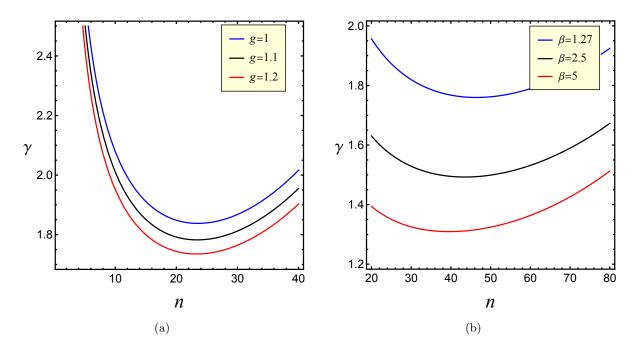


Figure 5: The relative growth factor γ as a function of the wave number n identified from the bifurcation condition (3.28), for different values of the pre-growth factor g and of the modulus ratio β , when $R_0 = 0.05$, $R_1 = 0.25$, $\zeta = 0.04$ ($h_0 = 0.01$), K = 20, and (a) $\beta = 1.27$ or (b) g = 1.1.

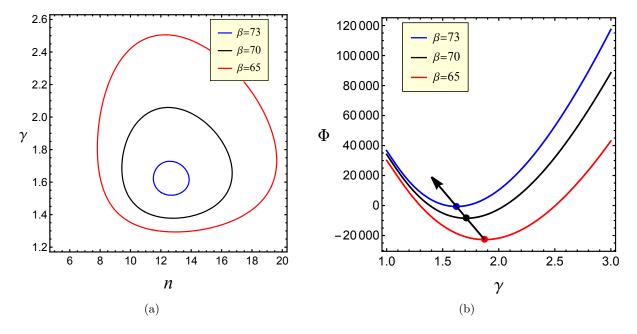


Figure 6: (a) The relative growth factor γ as a function of the wave number n identified from the bifurcation condition (3.28) when g = 1.1, $R_0 = 0.1$, $R_1 = 0.25$, $\zeta = 0.04$ ($h_0 = 0.01$), K = 20 and (b) the function Φ , given by equation (3.29), depending on the growth factor γ when the wave number is n = 12.

value of β for generating wrinkles. This optimal value can be identified by solving the simultaneous

equations:

$$\Phi = 0, \qquad \frac{\partial \Phi}{\partial n} = 0, \qquad \frac{\partial \Phi}{\partial \gamma} = 0.$$
(3.30)

where the bifurcation function Φ is described by equation (3.29). For the elephant trunk, the relevant results are those where β is close to 1.

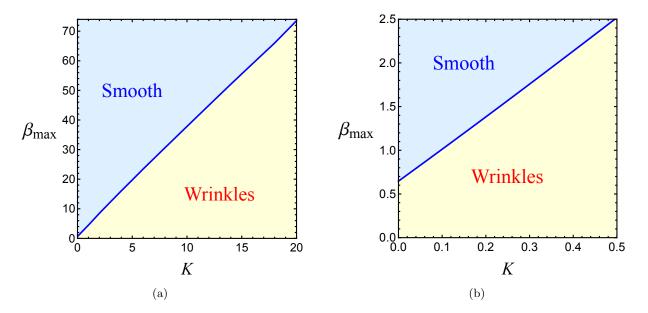


Figure 7: The maximum modulus ratio β_{max} as a function of the spring stiffness K when g = 1.1, $R_0 = 0.1$, $R_1 = 0.25$, and $\zeta = 0.04$ ($h_0 = 0.01$); (b) shows an enlarged detail of (a) for K close to 0.

Figure 7 displays the monotonically increasing β_{max} as a function of K. When $K \to 0$, corresponding to a free boundary, we find $\beta_{\text{max}} \approx 0.6466$. With a free end, if the skin modulus is higher or comparable to that for the muscle, so that $\beta \geq 1$, surface wrinkles are impossible, even when compression is generated by differential growth, i.e., when $\gamma > 1$. The underlying mechanism, in this case, is that growth happens through free trunk elongation. In the other limiting case, where $K \to \infty$, the spring constraint becomes a fixed end (Dirichlet boundary) condition, which is usually adopted in the context of growth-induced wrinkling (Jia et al., 2015). In this scenario, regardless of the value of β , surface wrinkles will form at a critical growth.

To investigate the effect of different parameters on the critical state, we set $\beta = 1.27$. Figure 8 shows how the critical relative growth factor and wave number vary with respect to the skin thickness h_0 . It suggests that a thicker skin always retards surface wrinkling and, at the same time, reduces the number of wrinkles. This is consistent with other reported results for growth-induced wrinkling (Goriely, 2017). Since $R_1 = 0.25$, a thicker skin layer will give rise to a lower curvature. As a result, we have that curvature increase will cause an earlier instability if the muscle thickness is fixed.

Next, we comment on the plots in Figure 9 showing the dependence of $\gamma_{\rm cr}$ and $n_{\rm cr}$ on the radius of the bilayer tube $R_1 + h_0$. In particular, we keep the thickness ratio $\zeta = h_0/R_1$ constant, meaning that both h_0 and R_1 will increase when $R_1 + h_0$ increases. It can be seen from Figure 9(a) that the critical differential growth $\gamma_{\rm cr}$ is non-monotonic but varies only in a small interval [2.099, 2.199]. Meanwhile, the critical wave number $n_{\rm cr}$ drops uniformly. This implies that, when the thickness ratio ζ is fixed, the critical differential growth does not alter much as the bilayer tube becomes thicker or thinner. However, the wave number changes rapidly. This may explain why there are more wrinkles in the distal narrower part of the elephant trunk than in the proximal wider part near

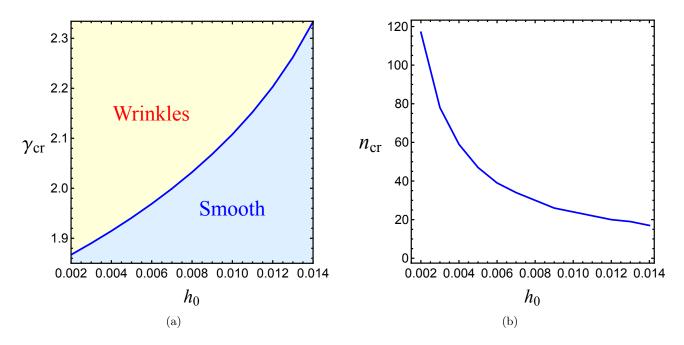


Figure 8: The critical (a) relative growth factor $\gamma_{\rm cr}$ and (b) wave number $n_{\rm cr}$ as functions of skin thickness h_0 when g = 1.1, $R_0 = 0.1$, $R_1 = 0.25$, K = 1, and $\beta = 1.27$.

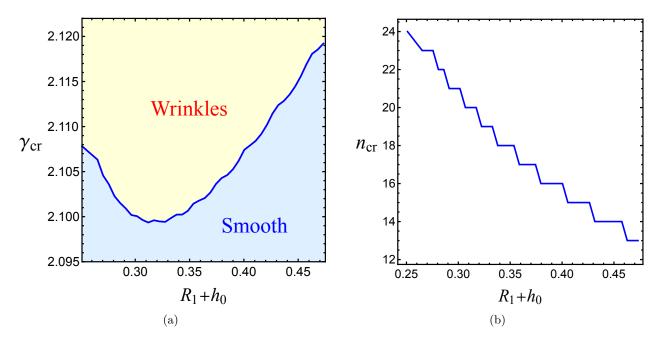


Figure 9: The critical (a) relative growth factor $\gamma_{\rm cr}$ and (b) wave number $n_{\rm cr}$ as functions of trunk outer radius $R_1 + h_0$ when g = 1.1, $R_0 = 0.1$, $\zeta = 0.04$, K = 1, and $\beta = 1.27$.

the skull (see Figure 1).

For planar film/substrate bilayers, surface wrinkles are usually not affected by the thickness of the substrate which can be seen as a half-space (Liu and Dai, 2014). To further check whether this is true for curved structures, we display the variations of $\gamma_{\rm cr}$ and $n_{\rm cr}$ as functions of R_1 by fixing all other parameters. As expected, R_1 alone has no effect on the wrinkled pattern but it does affect

the critical differential growth γ_{cr} . We find that a thicker muscle substrate will cause an earlier instability. Remember that, since h_0 is constant in this case, a higher R_1 corresponds to a lower curvature. Therefore, we summarize by stating that curvature increase can delay surface wrinkles if the thickness of the skin layer is fixed. Furthermore, we discover that the inner radius R_0 has no influence on both the critical differential growth and critical wave number, thus we do not show the associated results here.

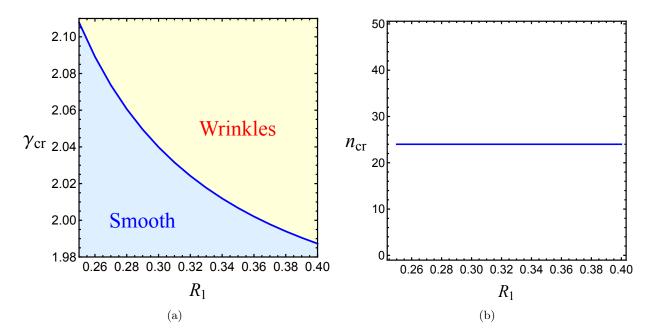


Figure 10: The critical (a) relative growth factor $\gamma_{\rm cr}$ and (b) wave number $n_{\rm cr}$ as functions of muscle substrate outer radius R_1 when g = 1.1, $R_0 = 0.1$, $\zeta = 0.1$, K = 1, and $\beta = 1.27$. In this case, the critical wave number is constant.

Figure 11 illustrates the effect of the spring stiffness K on the critical state, namely that the critical differential growth $\gamma_{\rm cr}$ decreases as K increases, while the critical wave number $n_{\rm cr}$ is a two-step function of K.

Finally, Figure 12 shows the critical relative growth factor $\gamma_{\rm cr}$ and wave number $n_{\rm cr}$ when the relative modulus β varies. In this case, we set K=20, instead of K=1 adopted in previous examples, since this latter value is too small to generate wrinkles when β is large. From Figure 7, we have $\beta_{\rm max}\approx 4.4746$ when K=1. However, if K=20, then the associated value becomes $\beta_{\rm max}\approx 73.5354$. So wrinkles are only possible provided that $\beta<\beta_{\rm max}$, as seen from Figure 7.

We observe from Figure 12(a) that the dependence of $\gamma_{\rm cr}$ on β is non-monotonic, which is different from the case when $K \to \infty$ (Jia et al., 2015; Liu et al., 2024). By carefully analyzing the deformation, we find that the bifurcation is induced by the resultant axial force N. By equation (2.25), N is proportional to both K and λ_z . When β increases, corresponding to a stiffer outer layer, a larger axial force N is required to generate an instability. Furthermore, Figure 12(b) shows the critical stretch $\lambda_z^{\rm cr}$ for bifurcation as a function of β . As an increasing function is obtained, more force is necessary to trigger surface wrinkling for higher β . In Figure 12(c), the critical wave number $n_{\rm cr}$ reduces with increasing β , consistent with the other results.

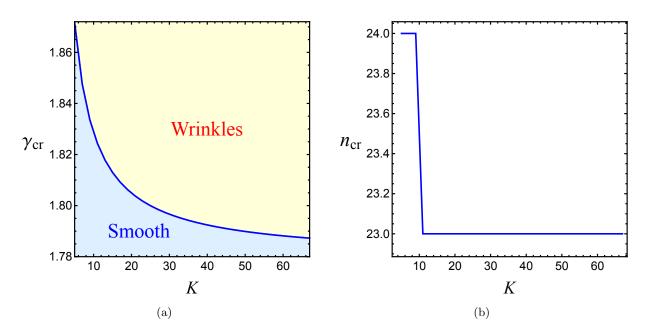


Figure 11: The critical (a) relative growth factor $\gamma_{\rm cr}$ and (b) wave number $n_{\rm cr}$ as functions of the spring stiffness K at the external boundary when g=1.1, $R_0=0.1$, $R_1=0.25$, $\zeta=0.04$ (h=0.01), and $\beta=1.27$. In this case, the critical wave number remains constant and equal to $n_{\rm cr}=23$ if K>10.

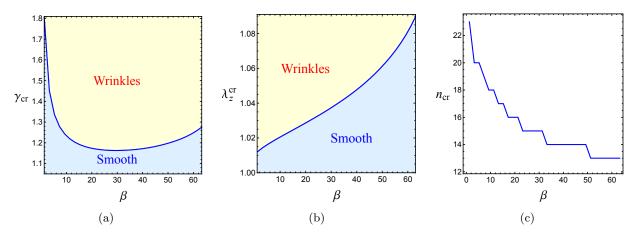


Figure 12: The critical (a) relative growth factor $\gamma_{\rm cr}$, (b) longitudinal stretch ratio $\lambda_z^{\rm cr}$ and (c) wave number $n_{\rm cr}$ as functions of the modulus ratio β when $g=1.1,\ R_0=0.1,\ R_1=0.25,\ \zeta=0.04$ ($h_0=0.01$), and K=20.

4 Asymptotic analysis

In this section, we present approximate analytical results for the primary deformation and the bifurcation condition.

4.1 Primary deformation

To make analytical progress, we set $\lambda_z = 1$, corresponding to the case with Dirichlet boundary conditions at both ends of the cylindrical system. This is also the limiting case when the elastic spring is infinitely stiff, i.e., $K \to \infty$. Given that the inner surface of the tubular system is free, the equation for the elastic hoop stretch α_{r_0} is

$$\frac{g}{\alpha_{r_0}^2} - \frac{g}{\alpha_{r_1}^2} + \beta \gamma^2 \frac{g}{\alpha_{r_1}^2} - \beta \gamma^2 \frac{g}{\alpha_h^2} + \log \frac{\alpha_{r_1}^2}{\alpha_{r_0}^2} + \beta \gamma \log \frac{\alpha_h^2}{\alpha_{r_1}^2} = 0, \tag{4.1}$$

where α_1^2 and α_h^2 depend on $\alpha_{r_0}^2$ through the relations (2.22). Assuming

$$\alpha_{r_0}^2 \sim g, \qquad \alpha_{r_1}^2 \sim g, \qquad \alpha_h^2 \sim g,$$

$$(4.2)$$

we have the Taylor expansion

$$\log \frac{\alpha_{r_1}^2}{\alpha_{r_0}^2} \approx \frac{\alpha_{r_1}^2}{\alpha_{r_0}^2} - 1, \qquad \log \frac{\alpha_h^2}{\alpha_{r_1}^2} \approx \frac{\alpha_h^2}{\alpha_{r_1}^2} - 1. \tag{4.3}$$

Then (4.1) is approximated as follows,

$$\frac{g}{\alpha_{r_0}^2} - \frac{g}{\alpha_{r_1}^2} + \beta \gamma^2 \frac{g}{\alpha_{r_1}^2} - \beta \gamma^2 \frac{g}{\alpha_h^2} + \frac{\alpha_{r_1}^2}{\alpha_{r_0}^2} - 1 + \beta \gamma \left(\frac{\alpha_h^2}{\alpha_{r_1}^2} - 1\right) = 0, \tag{4.4}$$

or equivalently,

$$\frac{\alpha_h^2}{g} \left(\frac{\alpha_{r_1}^2}{g} - \frac{\alpha_{r_0}^2}{g} \right) \left(\frac{\alpha_{r_1}^2}{g} + 1 \right) + \beta \gamma \frac{\alpha_{r_0}^2}{g} \left(\frac{\alpha_h^2}{g} - \frac{\alpha_{r_1}^2}{g} \right) \left(\frac{\alpha_h^2}{g} + \gamma \right) = 0. \tag{4.5}$$

Expressing α_1^2 and α_h^2 in terms of $\alpha_{r_0}^2$, as in (2.22), yields a cubic equation in $x = \alpha_{r_0}^2/g$, which admits only one real solution and can be solved directly. In particular, if $\gamma = 1$, then $\alpha_{r_0} = \alpha_{r_1} = \alpha_h = g^{1/2}$.

When $R_0 \sim h_0^{1/2}$, we can approximate $\alpha_{r_0} \sim g^{1/2}$ by seeking a solution of the form

$$\alpha_{r_0} \approx x_0 + x_1 h_0 + x_2 h_0^2 + x_3 h_0^3 + \cdots,$$
 (4.6)

where x_i , $i = 0, 1, 2, \dots$, are unknowns to be determined. After inserting the above formula into the cubic equation for $\alpha_{r_0}^2/g$, then expanding in powers of h_0 and collecting the coefficients of h_0^i , $i = 0, 1, 2, \dots$, we obtain infinitely many algebraic equations. Therefore we are able to solve for x_0 , x_1 , x_2 and find an asymptotic solution for $r_0 = \alpha_{r_0} R_0$ of the form

$$r_0 \approx g^{1/2} R_0 \left[1 + \frac{\beta \gamma h_0}{2R_1} \left(1 + \frac{8R_0^2}{R_1^2} \right) \left(\gamma^2 - 1 \right) + \frac{3\beta \gamma \left(\gamma^2 - 1 \right)^2 - 2 \left(4\gamma^2 - \gamma + 3 \right) (\gamma - 1)}{8R_1^2} \right]. \quad (4.7)$$

Note that $r_0 \to g^{1/2}R_0$ as $\gamma \to 1$, which is the exact solution when there is no differential growth, i.e., the skin and the muscle grow simultaneously at the same rate.

Figure 13 illustrates the exact and asymptotic solutions for r_0 as functions of the differential growth factor γ , when the pre-growth factor g and muscle outer radius R_1 are given, the inner radius is $R_0 = 0.1$, the skin thickness is $h_0 = 0.01$, and the relative stiffness is $\beta = 1.27$, as estimated in elephant trunk.

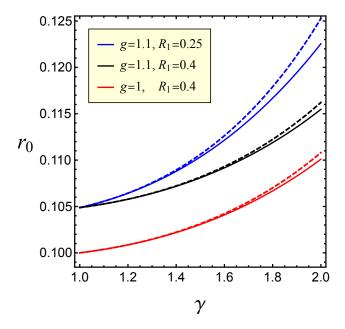


Figure 13: Comparisons between exact (solid) and asymptotic (dashed) solutions of r_0 as a function of the relative growth factor γ , for different values of g and R_1 , when $R_0 = 0.1$, $h_0 = 0.01$, and $\beta = 1.27$.

4.2 WKB approximation

To derive analytical formulae for the critical stretch and critical wave number, we employ the WKB (Wentzel-Kramers-Brillouin) method (Hinch, 1991), which has been found useful in the context of wrinkling in curved and graded structures (Jin et al., 2018; Jia et al., 2018; Liu et al., 2024).

First, we see from Figure 11(b) that the boundary spring stiffness K has a marginal influence on the critical wave number $n_{\rm cr}$. Therefore, we can assume $K \to \infty$, which is equivalent to $\lambda_z = 1$ (i.e., Dirichlet boundary conditions are imposed at both ends of the tubular system).

Second, we consider $\gamma=1$ so there is no differential growth, so that the pre-growth factor g as the control parameter. As the main purpose of the asymptotic analysis is to gain analytical insight into the effect of different geometrical and material parameters on the critical state, this is a reasonable simplification.

Then the primary deformation can be analytically characterized, as follows. Starting from the original eigenvalue problem arising from equations (3.14), we introduce a stream function

$$\psi(r,z) = f(r)\sin(kz). \tag{4.8}$$

Then the incremental displacements are

$$u(r,z) = \frac{1}{r} \frac{\partial \psi}{\partial z}, \qquad w(r,z) = -\frac{1}{r} \frac{\partial \psi}{\partial r},$$
 (4.9)

and the linearized incremental incompressibility condition is automatically satisfied.

In terms of the stream function, the incremental equations and boundary conditions become, respectively,

$$r^{3} \mathcal{A}_{1313} f'''' + 2r^{2} \left(r \mathcal{A}'_{1313} - \mathcal{A}_{1313} \right) f''' + a_{2}(r) f'' + a_{1}(r) f' + a_{0} f = 0, \tag{4.10}$$

and

$$\begin{cases}
\varrho_{s11}(r_1+h) = 0, & \varrho_{s31}(r_1+h) = 0, & \varrho_{m11}(r_0) = 0, & \varrho_{m31}(r_0) = 0, \\
\varrho_{s11}(r_1) = \varrho_{m11}(r_1), & \varrho_{s31}(r_1) = \varrho_{m31}(r_1), & f_s(r_1) = f_m(r_1), & f'_s(r_1) = f'_m(r_1),
\end{cases} (4.11)$$

where

$$\begin{cases}
\varrho_{11} = r^2 \mathcal{A}_{1313} f''' + \left(r^2 \mathcal{A}'_{1313} - r \mathcal{A}_{1313}\right) f'' + b_1(r) f' + b_0(r) f = 0, \\
\varrho_{31} = r \mathcal{A}_{1313} f'' - \mathcal{A}_{1313} f' + k^2 r \left(\mathcal{A}_{1313} + p\right) f = 0,
\end{cases}$$
(4.12)

with the coefficients $\{a_i\}_{i=0,1,2}$ and $\{b_i\}_{i=0,1}$ taking the following forms:

$$\begin{cases}
 a_{0} = k^{2}r \left(\mathcal{A}_{2222} - \mathcal{A}_{1111} + 2\mathcal{A}_{1133} - 2\mathcal{A}_{2233} + \mathcal{A}'_{1111} - \mathcal{A}'_{1122} - \mathcal{A}'_{1331} - \mathcal{A}'_{1133} + \mathcal{A}'_{2233} \right) \\
 + k^{4}r^{3}\mathcal{A}_{3131} + k^{2}r^{3}\mathcal{A}''_{1331} + k^{2}r^{3}p'', \\
 a_{1} = k^{2}r^{2} \left(\mathcal{A}_{1111} - 2\mathcal{A}_{1331} - 2\mathcal{A}_{1133} + \mathcal{A}_{3333} \right) + k^{2}r^{3} \left(2\mathcal{A}'_{1133} - \mathcal{A}'_{1111} + 2\mathcal{A}'_{1331} - \mathcal{A}'_{3333} \right) \\
 - 3\mathcal{A}_{1313} + 3r\mathcal{A}'_{1313} - r^{2}\mathcal{A}''_{1313}, \\
 a_{2} = k^{2}r^{3} \left(2\mathcal{A}_{1133} - \mathcal{A}_{1111} + 2\mathcal{A}_{1331} - \mathcal{A}_{3333} \right) + 3r\mathcal{A}_{1313} - 3r^{2}\mathcal{A}'_{1313} + r^{3}\mathcal{A}'_{1313}, \\
 b_{0} = k^{2}r \left(\mathcal{A}_{1111} - \mathcal{A}_{1122} - \mathcal{A}_{1133} + \mathcal{A}_{2233} + p + \mathcal{A}'_{1331} + p' \right), \\
 b_{1} = k^{2}r \left(2\mathcal{A}_{1133} - \mathcal{A}_{1111} + \mathcal{A}_{1331} - \mathcal{A}_{3333} - p' \right) + \mathcal{A}_{1313} - r\mathcal{A}'_{1313}.
\end{cases}$$

$$(4.13)$$

For the WKB-type solution to (4.10), we have

$$f = \exp\left(\int_{r_c}^r \mathcal{S}(\tau) d\tau\right),$$
 (4.14)

where S(r) is a function to be determined, the lower limit of integration is $r_c = r_1$ for the skin and $r_c = r_0$ for the muscle.

To solve the eigenvalue problem with variable coefficients, arising from the mathematical model for transverse wrinkles when the wave number $n = k/\pi$ is large, we look for solutions of the form

$$S(r) = nS_0(r) + S_1(r) + \frac{1}{n}S_2(r) + \cdots, \qquad (4.15)$$

where S_i $(i = 1, 2, 3, \cdots)$ are unknown functions.

Substituting the forms (4.14) and (4.15) into (4.10) then equating the coefficient of n to zero provides an algebraic equation for S_0 . Solving this equation directly yields four independent solutions. Similarly, we are able to derive S_1 and S_2 in a systematic manner.

For the neo-Hookean material and the restricted growth case considered here, namely, $\gamma = 1$ and $\lambda_z = 1$, we obtain the concise formulae given by

$$S_0^{(1,2)} = \pm \pi, \quad S_0^{(3,4)} = \pm \pi g^{-1/2}, \quad S_1^{(1,2,3,4)} = \frac{1}{2r}, \quad S_2^{(1,2)} = \pm \frac{3}{8\pi r^2}, \quad S_2^{(3,4)} = \pm \frac{3g^{1/2}}{8\pi r^2}. \quad (4.16)$$

As a result, we express the general solutions as follows

$$\begin{cases}
f_{\mathbf{m}}(r) = \sum_{i=1}^{4} C_{i} \exp\left(\int_{r_{0}}^{r} \mathcal{S}_{\mathbf{m}}^{(i)}(\tau) d\tau\right), & \text{for } r_{0} \leqslant r \leqslant r_{1}, \\
f_{\mathbf{s}}(r) = \sum_{i=1}^{4} C_{i+4} \exp\left(\int_{r_{1}}^{r} \mathcal{S}_{\mathbf{s}}^{(i)}(\tau) d\tau\right), & \text{for } r_{1} \leqslant r \leqslant r_{1} + h.
\end{cases}$$
(4.17)

Substituting these into the boundary and interface conditions (4.11), we obtain

$$\mathbf{MC} = \mathbf{0},\tag{4.18}$$

where

$$\mathbf{C} = [C_1, C_2, C_3, C_4, C_5, C_6, C_7, C_8]^{\mathrm{T}}, \tag{4.19}$$

and

$$\mathbf{M} = \begin{bmatrix} \mathbf{M}_{11} & \mathbf{M}_{12} \\ \mathbf{M}_{21} & \mathbf{M}_{22}, \end{bmatrix}, \tag{4.20}$$

with the sub-matrices

$$\mathbf{M}_{11} = \begin{bmatrix} 0 & 0 & 0 & 0 \\ 0 & 0 & 0 & 0 \\ \mathfrak{A}_{m1}(r_0) & \mathfrak{A}_{m2}(r_0) & \mathfrak{A}_{m3}(r_0) & \mathfrak{A}_{m4}(r_0) \\ \mathfrak{B}_{m1}(r_0) & \mathfrak{B}_{m2}(r_0) & \mathfrak{B}_{m3}(r_0) & \mathfrak{B}_{m4}(r_0) \end{bmatrix}, \tag{4.21}$$

$$\mathbf{M}_{12} = \begin{bmatrix} E_{s1} \mathfrak{A}_{s1}(r_1+h) & E_{s2} \mathfrak{A}_{s2}(r_1+h) & E_{s3} \mathfrak{A}_{s3}(r_1+h) & E_{s4} \mathfrak{A}_{s4}(r_1+h) \\ E_{s1} \mathfrak{B}_{s1}(r_1+h) & E_{s2} \mathfrak{B}_{s2}(r_1+h) & \mathfrak{B}_{s3}(r_1+h) & E_{s4} \mathfrak{B}_{s4}(r_1+h) \\ 0 & 0 & 0 & 0 \\ 0 & 0 & 0 & 0 \end{bmatrix}, \tag{4.22}$$

$$\mathbf{M}_{21} = \begin{bmatrix} -E_{m1}\mathfrak{A}_{m1}(r_1) & -E_{m2}\mathfrak{A}_{m2}(r_1) & -E_{m3}\mathfrak{A}_{m3}(r_1) & -E_{m4}\mathfrak{A}_{m4}(r_1) \\ -E_{m1}\mathfrak{B}_{m1}(r_1) & -E_{m2}\mathfrak{B}_{m2}(r_1) & -E_{m3}\mathfrak{B}_{m3}(r_1) & -E_{m4}\mathfrak{B}_{m4}(r_1) \\ -E_{m1} & -E_{m2} & -E_{m3} & -E_{m4} \\ -E_{m1}\mathcal{S}_{m}^{(1)'}(r_1) & -E_{m2}\mathcal{S}_{m}^{(2)'}(r_1) & -E_{m3}\mathcal{S}_{m}^{(3)'}(r_1) & -E_{m4}\mathcal{S}_{m}^{(4)'}(r_1) \end{bmatrix},$$
(4.23)

$$\mathbf{M}_{22} = \begin{bmatrix} \mathfrak{A}_{s1}(r_1) & \mathfrak{A}_{s2}(r_1) & \mathfrak{A}_{s3}(r_1) & \mathfrak{A}_{s4}(r_1) \\ \mathfrak{B}_{s1}(r_1) & \mathfrak{B}_{s2}(r_1) & \mathfrak{B}_{s3}(r_1) & \mathfrak{B}_{s4}(r_1) \\ 1 & 1 & 1 & 1 \\ \mathcal{S}_{s}^{(1)\prime}(r_1) & \mathcal{S}_{s}^{(2)\prime}(r_1) & \mathcal{S}_{s}^{(3)\prime}(r_1) & \mathcal{S}_{s}^{(4)\prime}(r_1) \end{bmatrix},$$
(4.24)

and the components

$$E_{mi} = \exp\left(\int_{r_0}^{r_1} \mathcal{S}_{m}^{(i)} dr\right), \quad E_{si} = \exp\left(\int_{r_1}^{r_1+h} \mathcal{S}_{s}^{(i)} dr\right),$$

$$\mathfrak{A}_{i} = b_0 + b_1 \mathcal{S}^{(i)\prime} + r\left(r\mathcal{A}'_{1313} - \mathcal{A}_{1313}\right) \left(\mathcal{S}^{(i)\prime}\right)^2 + r^2 \mathcal{A}_{1313} \left(\mathcal{S}^{(i)\prime}\right)^3 + r\left(r\mathcal{A}'_{1313} - \mathcal{A}_{1313}\right) \mathcal{S}_{s}^{(i)\prime\prime} + 3r^2 \mathcal{A}_{1313} \mathcal{S}_{s}^{(i)\prime\prime} \mathcal{S}_{s}^{(i)\prime\prime} + r^2 \mathcal{A}_{1313} \mathcal{S}_{s}^{(i)\prime\prime\prime},$$

$$\mathfrak{B}_{i} = rk^2 \left(\mathcal{A}_{1313} + p\right) - \mathcal{A}_{1313} \mathcal{S}^{(i)\prime} + r\mathcal{A}_{1313} \left(\mathcal{S}^{(i)\prime}\right)^2 + r\mathcal{A}_{1313} \mathcal{S}^{(i)\prime\prime},$$

$$(4.25)$$

Pursuing a non-trivial solution yields

$$\det \mathbf{M} = 0. \tag{4.26}$$

It can further to be deduced from (4.16) that $E_{\rm m1}$ and $E_{\rm m3}$ are exponentially large. On the other hand, as the skin is very thin, i.e., h is also small, $E_{\rm si}$, i=1,2,3,4, no longer possess the exponentially large or small nature. In view of these facts, the terms proportional to $E_{\rm m1}E_{\rm m3}$ are dominant such that

$$\frac{\det \mathbf{M}}{E_{\text{m1}}E_{\text{m3}}} = \Psi + \text{Exponentially Small Terms.} \tag{4.27}$$

We therefore obtain an approximate but explicit bifurcation condition:

$$\Psi(g, n, h_0, \beta, R_0, R_1) = 0. \tag{4.28}$$

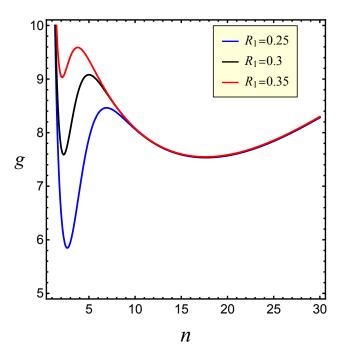


Figure 14: Exact bifurcation curves, for different values of the radius R_1 when $R_0 = 0.1$, $h_0 = 0.01$, $\beta = 1.27$, and $\gamma = 1$.

Before proceeding further, we specify the parameter values to be used in the subsequent calculations. To this end, we plot in Figure 14 the exact bifurcation curves, in the absence of relative growth (i.e., setting $\gamma = 1$), when the radius R_1 is fixed, $R_0 = 0.1$, $h_0 = 0.01$, and $\beta = 1.27$. We find that each curve has two local minima: a first one which increases as R_1 increases, with its critical wave number decreasing, and a second one which is independent of R_1 , and thus remains the same for all the curves. For example, when $R_1 = 0.25$, the first local minimum is the global minimum, attained at the wave number n = 2, while when $R_1 = 0.35$, the second local minimum is the global minimum attained at n = 17. This suggest a possible mode transition as the aspect ratio of the bilayer tube increases. Similar mode transitions have also been reported for compressed tubes (Goriely et al., 2008) and film/substrate structures (Liu and Dai, 2014; Dai and Liu, 2014).

For the current problem, we can determine the critical value for the geometric parameter R_1 where the mode transition occurs by applying the following two-step procedure:

(I) First, setting $R_1 = 0.35$ say, we determine g_{\min} and n_{\min} for the global minimum of the bifurcation curve by solving simultaneously the equations

$$\Phi(g,n) = 0, \qquad \frac{\partial \Phi(g,n)}{\partial n} = 0.$$
(4.29)

(II) Second, substituting $g = g_{\min}$ in the bifurcation condition Φ , we identify $R_1 = R_1^{(m)}$ and the

associated small wave number $n^{(m)}$ by solving the following two equations

$$\Phi(R_1, n) = 0, \qquad \frac{\partial \Phi(R_1, n)}{\partial n} = 0. \tag{4.30}$$

By applying the above procedure when $R_0 = 0.1$, $h_0 = 0.01$, $\beta = 1.27$ and $\gamma = 1$, as in Figure 14, we obtain $R_1^{(m)} \approx 0.2989$.

This interesting mode transition deserved to be treated in detail in a separate study. As our attention here is focused on wrinkling, i.e., on the case when the wave number is large, we shall select $R_1 = 0.4$ in all subsequent examples and thus avoid the above mode transition.

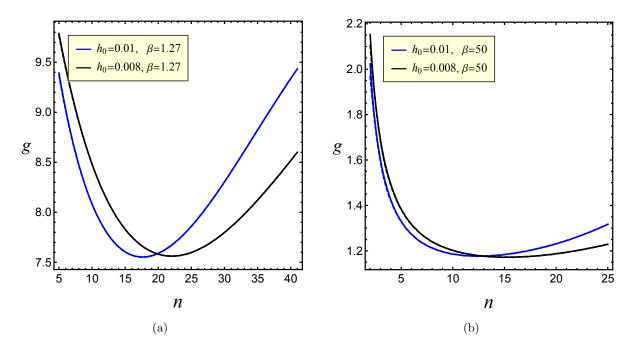


Figure 15: Comparisons between exact (solid) and asymptotic (dashed) bifurcation curves for different values of h_0 when $R_0 = 0.1$, $R_1 = 0.4$, $\gamma = 1$ and (a) $\beta = 1.27$ or (b) $\beta = 50$.

Figure 15 compares the exact and asymptotic bifurcation curves for the pre-growth factor g as a function of the wave number n, without differential growth (i.e., we set $\gamma = 1$), when the skin thickness h_0 is given, the muscle inner radius is $R_0 = 0.1$, its outer radius is $R_1 = 0.25$, and their modulus ratio is $\beta = 1.27$ (small) or $\beta = 50$ (large). Excellent agreement is found for all illustrated cases.

Next, we concentrate on two distinct limiting cases, namely when $\beta \sim 1$ and when $\beta \to \infty$, respectively.

4.2.1 The limiting case when the shear modulus ratio is close to unity

In elephant trunk, the skin and muscle substrate have comparable stiffness (Schulz et al., 2022a), thus $\beta \sim 1$. In this case, it can be seen from Figure 15(a) that the critical pre-growth factor $g_{\rm cr}$ is far from 1, even when the skin layer is very thin, i.e., $0 < h_0 \ll 1$. In this case, we have two small parameters h_0 and 1/n, and approximate the critical growth factor and critical wave number as follows, (Jia et al., 2018)

$$g_{\rm cr} = g_0 + g_1 h_0 + g_2 h_0^2 + \cdots (4.31)$$

and

$$n_{\rm cr} = h_0^{-1} \left(n_0 + n_1 h_0 + n_2 h_0^2 + \cdots \right).$$
 (4.32)

Inserting the above forms into the simultaneous equations given by the bifurcation condition (4.28) and the equation $\partial \Psi/\partial n = 0$, we find that the two leading order equations for g_0 and n_0 can only be solved numerically. Once they are solved, all higher order unknowns are then derived recursively. Although we do not include here the lengthy expressions for the leading-order equations and the recursive relations, we point out that g_0 and n_0 are both independent of R_0 and R_1 , and are only related to β , indicating that the critical pre-growth $g_{\rm cr}$ is dominated by β only. This is useful in explaining Figure 9(a) where $\gamma_{\rm cr}$ belongs in the small interval [2.099, 2.199]. Similarly, $n_{\rm cr}h_0$ is governed by β , and thus the critical wave number $n_{\rm cr}$ decreases as h_0 increases, which explains the result in Figure 9(b).

The three-term approximations (4.31)-(4.32) for the critical pre-growth factor $g_{\rm cr}$ and critical wave number $n_{\rm cr}$ when $R_0 = 0.1$, $R_1 = 0.4$, and $\zeta = 0.0025$ ($h_0 = 0.01$) are compared with the exact solutions in Figure 16. It can be seen from these plots that, for β close to 1, an excellent agreement is found, validating our asymptotic solutions.

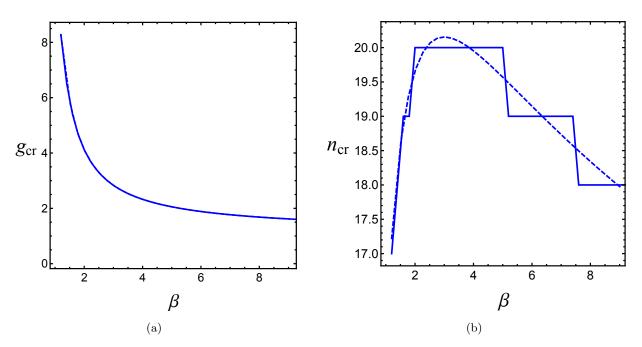


Figure 16: Comparisons between exact (solid) and asymptotic (dashed) solutions for the critical pre-growth factor $g_{\rm cr}$ and critical wave number $n_{\rm cr}$ when $R_0 = 0.1$, $R_1 = 0.4$, $\zeta = 0.0025$ ($h_0 = 0.01$), and $\gamma = 1$.

4.2.2 The limiting case when the shear modulus ratio is large

When the modulus ratio β is large, we observe from Figure 15(b) that the critical pre-growth factor is close to 1. So there are in total four small parameters, namely, $g_{\rm cr} - 1$, $1/\beta$, 1/n, and h_0 . Again, we assume that there is no differential growth, i.e., $\gamma = 1$. To derive analytical formulae for the critical stretch and critical wave number, we set the scalings (Liu and Dai, 2014; Jin et al., 2018)

$$g_{\rm cr} - 1 \sim \mathcal{O}\left(\beta^{-2/3}\right), \qquad n_{\rm cr} \sim \mathcal{O}\left(\beta^{2/3}\right), \qquad h_0 \sim \mathcal{O}\left(\beta^{-1}\right),$$
 (4.33)

then pursue an asymptotic solution in terms of the small parameter $1/\beta$. In a similar manner as in the previous subsection, we obtain the following explicit forms for the critical pre-growth factor

$$g_{\rm cr} = 1 + 3^{2/3}\beta^{-2/3} + \frac{7}{20}3^{4/3}\beta^{-4/3} + \frac{h_0^2}{R_1^2}3^{1/3}\beta^{2/3} - \frac{h_0}{2R_1}\beta^{-1} + \frac{1}{2}3^{2/3}\beta^{-5/3} + \frac{1009}{2800}3\beta^{-2} + \frac{79h_0^2}{20R_1^2} - \frac{h_0^4}{R_1^4}\beta^2 + \mathcal{O}\left(\beta^{-7/3}\right),$$

$$(4.34)$$

and the critical wave number

$$n_{\rm cr} = \frac{1}{\pi h_0} \left[3^{1/3} \beta^{-1/3} - \frac{1}{20} 3^3 \beta^{-1} + \frac{h_0^2}{R_1^2} \beta - \frac{h_0}{2R_1} 3^{-1/3} \beta^{-2/3} + \frac{47h_0^2}{40R_1^2} 3^{-1/3} \beta^{1/3} - \frac{2h_0^4}{R_1^4} 3^{-1/3} \beta^{7/3} + \frac{1229}{2900} 3^{2/3} \beta^{-5/3} + \mathcal{O}\left(\beta^{-1}\right) \right].$$

$$(4.35)$$

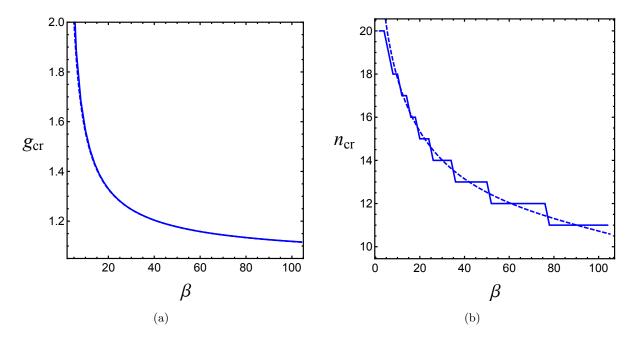


Figure 17: Comparisons between exact (solid) and asymptotic (dashed) solutions for the critical pre-growth factor $g_{\rm cr}$ and critical wave number $n_{\rm cr}$ when $R_0 = 0.1$, $R_1 = 0.4$, $\zeta = 0.025$ ($h_0 = 0.01$), and $\gamma = 1$.

From equations (4.34)-(4.35) we infer that the inner radius R_0 is not involved up to the truncated order. Meanwhile, the muscle radius R_1 and the skin thickness h_0 affect the critical pre-growth factor trough higher order terms, indicating that their influence is relatively minor compared to that of the relative modulus β . In addition, both h_0 and β feature in the leading-order term in (4.35). Recalling the notation $\zeta = h_0/R_1$, we can rewrite

$$g_{\rm cr} = 1 + 3^{2/3}\beta^{-2/3} + \frac{7}{20}3^{4/3}\beta^{-4/3} + \zeta^2 3^{1/3}\beta^{2/3} - \frac{1}{2}\zeta\beta^{-1} + \frac{1}{2}3^{2/3}\beta^{-5/3} + \frac{1009}{2800}3\beta^{-2} + \frac{79}{20}\zeta^2 - \zeta^4\beta^2 + \mathcal{O}\left(\beta^{-7/3}\right),$$

$$(4.36)$$

and

$$n_{\rm cr} = \frac{1}{\pi h_0} \left[3^{1/3} \beta^{-1/3} - \frac{1}{20} 3^3 \beta^{-1} + \zeta^2 \beta - \frac{\zeta}{2} 3^{-1/3} \beta^{-2/3} + \frac{47}{40} \zeta^2 3^{-1/3} \beta^{1/3} - 2\zeta^4 3^{-1/3} \beta^{7/3} + \frac{1229}{2900} 3^{2/3} \beta^{-5/3} + \mathcal{O}\left(\beta^{-1}\right) \right].$$

$$(4.37)$$

It can be seen from the above equations that $g_{\rm cr}$ and $n_{\rm cr}\pi h_0$ depend h_0 and R_1 through ζ . In particular, when β and ζ are fixed, the critical pre-growth factor $g_{\rm cr}$ is constant.

Figure 17 shows the exact and asymptotic solutions for the critical pre-growth factor $g_{\rm cr}$ given by equation (4.36) and the critical wave number $n_{\rm cr}$ given by equation (4.37), as functions of the modulus ratio β , when $R_0 = 0.1$, $R_1 = 0.4$, and $\zeta = 0.04$ ($h_0 = 0.01$), in the absence of differential growth (i.e., when $\gamma = 1$).

We also remark that, in equation (4.37) for transverse wrinkles distributed along the tube length, the leading-order term $3^{1/3}\beta^{-1/3}$ is the same as those for the circumferential wrinkles in growing bilayer tubes (Jin et al., 2018), core/shell cylinders (Jia et al., 2018), and surface wrinkles in planar film/substrate bilayers (Liu et al., 2024). This analysis further confirms the universal scaling between the modulus ratio and number of wrinkles.

5 Conclusion

This work stems from the need to understand wrinkling in elephant trunk where physical measurements suggest that skin and muscle substrate have comparable stiffness. Due to their mechanical compatibility, the two components can grow together seamlessly, and the wrinkled skin acts as a protective barrier that is at the same time thicker and more flexible than the unwrinkled skin. Moreover, geometric parameters, such as curvature, play key roles in the formation of transverse wrinkles. In particular, our model predicts that fewer wrinkles form and earlier in the proximal region where curvature is lower than in the distal region which has larger curvature, as observed in elephant trunks. Similarly, the dorsal side presents more wrinkling than the ventral side, since curvature is higher dorsally than ventrally.

While our theoretical and numerical results describe mathematically how transverse wrinkles form, our investigation extends beyond that and can be useful to many other applications. Follow-up models should take into account additional deformations and loading conditions, e.g., bending, unbending, and inflation under internal pressure, as in a water filled elephant trunk, for example. More sophisticated hyperelastic strain-energy functions for skin and muscle tissues could also be considered.

The elephant trunk is a rich source of inspiration for bio-mechanical devices, but its physiology is yet to be understood. We hope that our analysis will stimulate further quantitative studies of elephant trunk and elephant skin more generally.

Acknowledgment We gratefully acknowledge the UKRI Horizon Europe Guarantee MSCA (Marie Skłodowska-Curie Actions) Postdoctoral Fellowship to Yang Liu (EPSRC Grant No. EP/Y030559/1). Yang Liu further acknowledges the financial support from the National Natural Science Foundation of China (Project No. 12072227).

Data availability statement There are no additional data associated with this article.

Conflict of interest The authors have no competing interests to declare that are relevant to the content of this article.

References

- Ayer AA, Mariappa D. 1950. External characters of three foetuses of the Indian elephant. Proceedings of the Indian Academy of Sciences B 31(4), 193–209 (doi: 10.1007/BF03050577).
- Ben Amar M., Goriely A., 2005. Growth and instability in elastic tissues. Journal of the Mechanics and Physics of Solids 53, 2284–2319 (doi: 10.1016/j.jmps.2005.04.008).
- Biryukov, S.V., 1985. Impedance method in the theory of elastic surface waves. Sov. Phys. Acoust. 31, 350–354.
- Birykov, S.V., Gulyaev, Y.V., Krylov, V.V., Plessky, V.P., 1995. Surface acoustic waves in inhomogeneous media. Springer Berlin, Heidelberg.
- Boas J.E.V., Paulli S., 1908. The Elephant's Head: Studies in the Comparative Anatomy of the Organs of the Head of the Indian Elephant and Other Mammals, published at the cost of the Carlsberg-Fund, Copenhagen.
- Dagenais P., Hensman S., Haechler V., 2021. Elephants evolved strategies reducing the biomechanical complexity of their trunk. Current Biology 31(21), 4727—4737 (doi: 10.1016/j.cub.2021.08.029).
- Dai, H.-H., Liu, Y., 2014. Critical thickness ratio for buckled and wrinkled fruits and vegetables. Europhysics Letters 108(4), 44003 (doi: 10.1209/0295-5075/108/44003).
- De Pascalis R., Destrade M., Goriely A., 2010. Nonlinear correction to the Euler buckling formula for compressed cylinders with guided-guided end conditions. Journal of Elasticity 102 (2), 191–200 (doi: 10.1007/s10659-010-9265-6).
- Destrade M., Ogden R.W., Sgura I., Vergori L., 2014. Straightening wrinkles, Journal of the Mechanics and Physics of Solids 65, 1–11 (doi: 10.1016/j.jmps.2014.01.001).
- Duka E.D., England A.H., Spencer A.J.M., 1993. Bifurcation of a solid circular cylinder under finite extension and torsion. Acta Mechanica 98, 107–121 (doi: 10.1007/BF01174297).
- Eales NB. 1926. XI—The Anatomy of the head of a foetal African elephant, Elephas africanus (Loxodonta africana). Transactions of the Royal Society of Edinburgh 54(3), 491–551. (doi: 10.1017/S0080456800016082).
- Emery D., Fu Y., 2021. Elasto-capillary circumferential buckling of soft tubes under axial loading: existence and competition with localised beading and periodic axial modes. Mechanics of Soft Materials 3, 3 (doi: 10.1007/s42558-021-00034-x).
- Flügge W., 1962. Statik und Dynamik der Schalen. Berlin, Springer.
- Flügge W., 1963. Stresses in Shells. Berlin, Heidelberg, New York, Springer-Verlag.
- Fosdick R.A., Shield R.T., 1963. Small bending of a circular bar superposed on finite extension or compression. Archive for Rational Mechanics and Analysis 12, 223–248 (doi: 10.1007/BF00281227).
- Fu Y., Liu J.L., Francisco G.S., 2016. Localized bulging in an inflated cylindrical tube of arbitrary thickness the effect of bending stiffness. Journal of the Mechanics and Physics of Solids 90, 45–60 (doi: 10.1016/j.jmps.2016.02.027).

- Fu Y., Jin L., Goriely A., 2021. Necking, beading, and bulging in soft elastic cylinders. Journal of the Mechanics and Physics of Solids 147, 104250 (doi: 10.1016/j.jmps.2020.104250).
- Goriely A., 2017. The Mathematics and Mechanics of Biological Growth, Springer-Verlag, New York.
- Goriely A., Vandiver R., Destrade M., 2008. Nonlinear Euler buckling. Proceedings of the Royal Society A 464(2099), 3003–3019 (doi:10.1098/rspa.2008.0184).
- Green A.E., Rivlin R.S., Shield R.T., 1952. General theory of small elastic deformations superposed on finite elastic deformations. Proceedings of the Royal Society A 211, 128–154 (doi: 10.1098/rspa.1952.0030).
- Gustafson K., Abe T., 1998. The third boundary condition Was it Robin's?. The Mathematical Intelligencer 20, 63–71 (doi: 10.1007/BF03024402).
- Hildebrandt T., Drews B., Gaeth A.P., Goeritz F., Hermes R., Schmitt D., Gray C., Rich P., Streich W.J., Short R.V., Renfree M.B., 2007. Foetal age determination and development in elephants. Proceedings of the Royal Society B 274, 323–331 (doi: 10.1098/rspb.2006.3738).
- Hinch, E.J., 1991. Perturbation Methods. Cambridge University Press.
- Il'ichev A.T., Fu Y., 2014. Stability of an inflated hyperelastic membrane tube with localized wall thinning. International Journal of Engineering Science 80, 53–61 (doi: 10.1016/j.ijengsci.2014.02.031).
- Jia F., Cao Y.P., Zhao Y., Feng X.Q., 2014. Buckling and surface wrinkling of an elastic graded cylinder with elastic modulus arbitrarily varying along radial direction. International Journal of Applied Mechanics 6(1), 1450003 (doi: 10.1142/S1758825114500033).
- Jia F., Li B., Cao Y.P., Xie W.H., Feng X.Q., 2015. Wrinkling pattern evolution of cylindrical biological tissues with differential growth. Physical Review E 91(1), 012403 (doi: 10.1103/Phys-RevE.91.012403).
- Jia F., Pearce S.P., Goriely A., Curvature delays growth-induced wrinkling. Physical Review E 98, 033003 (doi: 10.1103/PhysRevE.98.033003).
- Jin L., Liu Y., Cai Z., Asymptotic solutions on the circumferential wrinkling of growing tubular tissues. International Journal of Engineering Science 128, 31–43 (doi: 10.1016/j.ijengsci.2018.03.005).
- Kaczmarski B., Leanza S., Zhao R., Kuhl E., Moulton D.E., Goriely A., 2024. Minimal design of the elephant trunk as an active filament. Physical Review Letters 132, 248402 (doi: 10.1103/Phys-RevLett.132.248402).
- Kaczmarski B., Moulton D.E., Goriely A., Kuhl E., 2024. Minimal activation with maximal reach: Reachability clouds of bio-inspired slender manipulators. Extreme Mechanics Letters Volume 71, 102207 (doi: 10.1016/j.eml.2024.102207).
- Kier W.M., Smith K.K., 1985. Tongues, tentacles and trunks: The biomechanics of movement in muscular-hydrostats. Zoological Journal of the Linnean Society 83(4), 307—324 (doi: 10.1111/j.1096-3642.1985.tb01178.x).

- Leanza S., Lu-Yang J., Kaczmarski B., Wu S., Kuhl E., Zhao R.R., 2024. Elephant trunk inspired multimodal deformations and movements of soft robotic arms. Advanced Functional Materials, 202400396 (doi: 10.1002/adfm.202400396).
- Li R.C.M., Yen K.H., 1972. Elastic waves guided by a solid layer between adjacent substrates. IEEE Transactions on Microwave Theory and Techniques 20(7), 477–486 (doi: 10.1109/TMTT.1972.1127788).
- Liu Y., Dai H.-H., 2014. Compression of a hyperelastic layer-substrate structure: Transitions between buckling and surface modes. International Journal of Engineering Science 80, 74–89 (doi: 10.1016/j.ijengsci.2014.02.020).
- Liu Y., Dorfmann L., 2024. Localized necking and bulging of finitely deformed residually stressed solid cylinder. Mathematics and Mechanics of Solids 29(6), 1153–1175 (doi: 10.1177/10812865231186951).
- Liu C., Du Y., Li K., Zhang Y., Han Z., Zhang Y., Qu S., Lü C., 2022. Geometrical incompatibility guides pattern selection in growing bilayer tubes. Journal of the Mechanics and Physics of Solids 169, 105087 (doi: 10.1016/j.jmps.2022.105087).
- Liu R.-C., Liu Y., Goriely A., 2024. Surface wrinkling of a film coated to a graded substrate. Journal of the Mechanics and Physics of Solids, 186, 105603 (doi: 10.1016/j.jmps.2024.105603).
- Pearce S.P., Fu Y., 2010. Characterization and stability of localized bulging/necking in inflated membrane tubes. IMA Journal of Applied Mathematics 75(4), 581–602 (doi: 10.1093/ima-mat/hxq026).
- Schulz A.K., Fourney E., Sordilla S., Sukhwani A., Hu D.L., 2020. Elephant trunk skin: Nature's flexible kevlar. International Conference on Intelligent Robots and Systems (IROS), 10.
- Schulz A.K., Boyle M., Boyle C., Sordilla S., Rincon C., Hooper S., Aubuchon C., Reidenberg J.S., Higgins. C, Hu D.L., 2022. Skin wrinkles and folds enable asymmetric stretch in the elephant trunk. PNAS Biophysics and Computational Biology 119(31), e2122563119 (doi: 10.1073/pnas.2122563119).
- Schulz A.K., Reidenberg J.S., Wu J.N., Tang C.Y., Seleb B., Mancebo J., Elgart N., Hu D.L., 2022. Elephants trunks use an adaptable prehensile grip. Bioinspiration & Biomimetics 18, 026228 (doi: 10.1088/1748-3190/acb477).
- Schulz A.K., Schneider N., Zhang M., Singal K., 2023. A year at the forefront of hydrostatic motion. Biology Open 12, bio059834 (doi: 10.1242/bio.059834).
- Schulz A.K., Reveyaz N., Kaufmann L., Ritter C., Hildebrandt T., Brecht M., 2023. Elephants develop wrinkles through both form & function. Society of Integrative and Comparative Biology, Seattle, USA, 1 (doi: 10.1101/2023.08.24.554618).
- Shuvalov, A.L., 2003. A sextic formalism for three-dimensional elastodynamics of cylindrically anisotropic radially inhomogeneous materials. Proc. R. Soc. Lond. A 459, 1611–1639.
- Shuvalov, A.L., 2003. The frobenius power series solution for cylindrically anisotropic radially inhomogeneous elastic materials. Q. J. Mech. Appl. Math, 56(3), 327–345.

- Sigaeva T., Mangan R., Vergori L., Destrade M., Sudak L., 2018. Wrinkles and creases in the bending, unbending and eversion of soft sectors. Proceedings of the Royal Society A 474, 20170827 (doi: 0.1098/rspa.2017.0827).
- Springhetti R., Rossetto G., Bigoni D., 2023. Buckling of thin-walled cylinders from three dimensional nonlinear elasticity. Journal of Elasticity 154(1-4), 297–323 (doi: 10.1007/s10659-022-09905-4).
- Stroh A.N., 1962. Steady state problems in anisotropic elasticity. Journal of Mathematics and Physics 41, 77–103 (doi: 10.1002/sapm196241177).
- Thompson D.W., 1942. On Growth and Form, Cambridge University Press, Cambridge.
- Trivedi D., Rahn C.D., Kier W.M., Walker I.D., 2008. Soft robotics: biological inspiration, state of the art, and future research. Applied Bionics and Biomechanics 5(3), 99–117 (doi: 10.1080/11762320802557865).
- Wang M., Fu Y., 2021. Necking of a hyperelastic solid cylinder under axial stretching: Evaluation of the infinite-length approximation. International Journal of Engineering Science 159, 103432 (doi: 10.1016/j.ijengsci.2020.103432).
- Wang S.B., Guo G.M., Zhou L., Li L.A., Fu Y., 2019. An experimental study of localized bulging in inflated cylindrical tubes guided by newly emerged analytical results. Journal of the Mechanics and Physics of Solids 124, 536–554 (doi: 10.1016/j.jmps.2018.11.011).
- Wilkes E.W., 1955. On the stability of a circular tube under end thrust. The Quarterly Journal of Mechanics and Applied Mathematics 8, 88–100 (doi:10.1093/qjmam/8.1.88).
- Wilson JF, Mahajan U, Wainwright SA, Croner LJ. 1991. A continuum model of elephant trunks. ASME Journal of Biomechanical Engineering 113(1), 79–84 (doi: 10.1115/1.2894088).
- Woo T.C., Shield R.T., 1962. Fundamental solutions for small deformations superposed on finite biaxial extension of an elastic body. Archive for Rational Mechanics and Analysis 9, 196–224 (doi: 10.1007/BF00253345).
- Wu W., Yin Y., Li Y., Fan X., 2024. Theoretical analysis of inflated tube wrinkling behavior under pure bending. International Journal of Mechanical Sciences 273, 109166 (doi: 10.1016/j.ijmecsci.2024.109166).
- Ye Y., Liu Y., Fu Y., 2020. Weakly nonlinear analysis of localized bulging of an inflated hyperelastic tube of arbitrary wall thickness. Journal of the Mechanics and Physics of Solids 135, 103804 (doi: 10.1016/j.jmps.2019.103804).
- Ye S., Yin S.F., Li B., Feng X.Q., 2019. Torsion instability of anisotropic cylindrical tissues with growth. Acta Mechanica Solida Sinica 32(5), 621–632 (doi: 10.1007/s10338-019-00087-6).
- Zhang J., Li Y., Kan Z., Yuan Q., Rajabi H., Wu Z., Peng H., Wu J., 2023. A preprogrammable continuum robot inspired by elephant trunk for dexterous manipulation. Soft Robotics 10(3), 636-646 (doi: 10.1089/soro.2022.0048).
- Zhao Y., Cao Y.P., Feng X.Q., Ma K., 2014. Axial compression-induced wrinkles on a core–shell soft cylinder: Theoretical analysis, simulations and experiments. Journal of the Mechanics and Physics of Solids 73, 212–227 (doi: 10.1016/j.jmps.2014.09.005).

Zhu Y., Luo X.Y., Ogden R.W., 2008. Asymmetric bifurcations of thick-walled circular cylindrical elastic tubes under axial loading and external pressure. International Journal of Solids and Structures 45, 3410–3429 (doi: 10.1016/j.ijsolstr.2008.02.005).